Three-Dimensional Spectroscopy of Vibrational Energy in Liquids: Nitromethane and Acetonitrile

ARTICLE *in* THE JOURNAL OF PHYSICAL CHEMISTRY B · JULY 2013

Impact Factor: 3.3 · DOI: 10.1021/jp405197g · Source: PubMed

3 AUTHORS, INCLUDING:

Dana D Dlott
University of Illinois, Urbana-Champaign
297 PUBLICATIONS **6,621** CITATIONS

SEE PROFILE

THE JOURNAL OF PHYSICAL CHEMISTRY B

Article

pubs.acs.org/JPCB

Three-Dimensional Spectroscopy of Vibrational Energy in Liquids: Nitromethane and Acetonitrile

Yuxiao Sun, Brandt C. Pein, and Dana D. Dlott*

School of Chemical Sciences, University of Illinois at Urbana—Champaign, Urbana, Illinois 61801, United States

ABSTRACT: We introduce a novel type of three-dimensional (3D) spectroscopy to study vibrational energy transfer, where an IR pulse tunable through the CH-stretching and CD-stretching regions was used to create parent vibrational excitations in liquids and a visible probe pulse was used to generate both Stokes and anti-Stokes Raman spectra as a function of delay time. The Raman spectra determine how much vibrational excitation was present in each probed state. The three dimensions are the wavenumber of the pumped state, the wavenumber of the probed state, and the time interval. The technique was used to study nitromethane (NM) and acetonitrile (ACN) and their deuterated analogues at ambient temperature. The 3D spectra were quite complicated. Three types of artifacts due to nonlinear light scattering were observed. Along the diagonal were two fundamental CH-stretch (or CD-stretch) transitions and several weaker combination bands or overtone transitions. Because Raman spectroscopy allows us to simultaneously probe a wide wavenumber region, for every diagonal peak, there were ~10 off-diagonal peaks. The cross-peaks at shorter delay times reveal the nature of the initial excitation by showing which lower-wavenumber excitations were produced along with the pumped CH-stretch or CD-stretch. The longer-time spectra characterized vibrational energy relaxation processes, and showed how daughter vibrations were generated by different parent excitations.

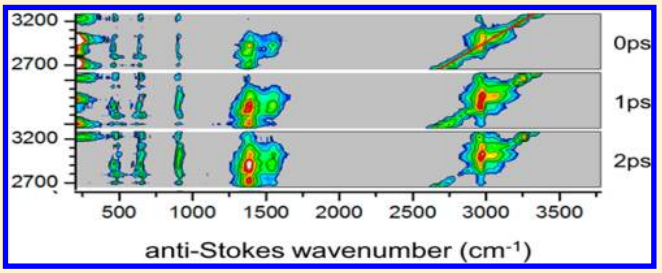

1. INTRODUCTION

The IR-Raman method is a three-dimensional (3D) technique[1] to study vibrational energy transfer (VET), and it is most commonly used to study liquids.[2−7] The three dimensions are pump wavenumber, probe wavenumber, and delay time, so a 3D IR-Raman spectrum shows how vibrational energy initially deposited in parent molecular vibrations by tunable IR pulses is redistributed to the other daughter vibrations in time t. The vibrations are probed with visible pulses that generate both Stokes and anti-Stokes Raman spectra, to quantitatively determine the vibrational energy in every probed mode. Both laser pulses are semi-impulsive,[1] so the durations are long enough (and the bandwidths small enough) to selectively pump and probe individual vibrational transitions but short enough to resolve vibrational energy relaxation (VR) lifetimes T_1. In a 3D spectrum, energy flow out of a parent vibration is observed on the diagonal, and excited daughter states generated by VET from a parent are observed off the diagonal. After the parent energy has been transferred to successive generations of daughter vibrations, a thermalized state will eventually be achieved.

In previous works from our group and others, the dimension of pump wavenumber has not been explored thoroughly. Most published studies looked at molecular responses at one or two pump wavenumbers, and did not investigate in detail the effects of varying the pump wavenumber. In fact, in early IR-Raman studies of ethanol[8] and methyl iodide,[2] among others,[9,10] which had multiple CH-stretch transitions but were studied at only one pump wavenumber, it was asserted that there was fast redistribution between all parent CH-stretch excitations, so any pump wavenumber in the C−H stretch region would produce the same result. One problem with this picture was that the nature of the fast redistribution was never specified. For instance, it might involve uniform excitation of all CH-stretch excitations or perhaps a thermal equilibrium among those excitations. The idea of pump-wavenumber independent dynamics was disproved in a 2000 study from our group,[11] where the CH-stretch transitions of methanol were excited at two different IR wavenumbers. However, until recently, laser technology did not support the laborious measurement of IR-Raman spectra over a broad continuous range of IR pump wavenumbers. The best example of 3D IR-Raman spectroscopy was a previous study of Iwaki and co-workers, where methanol was studied at two pump wavenumbers in the CH-stretch region and two pump wavenumbers in the OH-stretch region.[1] Recently, we added a computer-controlled apparatus for continuous tuning of the IR pump pulses, and presented results on nitrobenzene,[12] where the IR pulses were continuously tuned through the 2500−3500 cm^{-1} range. The full 3D nature of VET in nitrobenzene was not fully realized, since only a few delay times were probed in those experiments.

In the present work, we present three-dimensional data sets for nitromethane (NM) and acetonitrile (ACN) and their fully

Special Issue: Michael D. Fayer Festschrift

Received: May 26, 2013
Revised: July 2, 2013

   dx.doi.org/10.1021/jp405197g | J. Phys. Chem. B XXXX, XXX, XXX−XXX

deuterated analogues d_3-NM and d_3-ACN. The NM, d_3-NM, and ACN have been the subject of previous studies from our laboratory,[4,13−17] where VET pathways of each liquid were studied using two different pump wavenumbers. The novel feature of the present study is the acquisition of complete 3D data sets on the previously studied liquids, along with the first results on d_3-ACN. Here we will not concentrate on describing the detailed VET pathways, although that information is clearly present in the 3D spectra. Instead we will focus on the nature of 3D IR-Raman spectroscopy, and how the patterns evident in 3D spectra can be used to understand vibrational excitation dynamics in these different liquids.

In the liquids studied here, the parent excitations were in spectrally congested regions where fundamental CH-stretches or CD-stretches lie on top of and may be mixed with combinations and overtones of lower-energy modes. Understanding the admixture of excitations that comprise a parent state is possible because, in IR-Raman spectroscopy, those excitations appear as excitations of the underlying fundamental transitions. The anharmonic shifts associated with combination bands are generally not detectable because they are usually less than the probe laser bandwidth. For a concrete example, in NM, the combination band excitation $\nu_a(NO_2) + \nu_s(NO_2)$ near 2950 cm^{-1} would appear at shorter delay times (t = 0, 1 ps) as excitation of ∼1562 cm^{-1} $\nu_a(NO_2)$ and ∼1402 cm^{-1} $\nu_s(NO_2)$.[17]

An important property of our IR-Raman technique is that the spectra have an increased sensitivity to weaker IR transitions, so weaker overtone and combination-band transitions will be enhanced relative to stronger resonant IR transitions such as CH-stretch. This is a consequence of the experimental arrangement and the different optical penetration depths of the pump and probe pulses.[4] In the IR-Raman experiment, the anti-Stokes signals from IR pulses at an absorption peak and in an absorption valley can be the same intensity. The Raman probe pulses are nonresonant and probe the entire ∼50 μm thick sample. As long as the IR penetration depth is less than the sample thickness, all the IR photons will be absorbed and the number of excitations that generate the anti-Stokes signals will remain constant. It is only when the IR pulses are tuned to a region where the absorption is weak enough that the absorption depth becomes comparable to the sample thickness that the number of probed excitations begins to decrease.[4]

The decay of the parent excitation occurs by dissipative VET processes that ultimately lead to a bulk temperature jump ΔT that are best observed at t > 1 ps.[4−6] Dissipation results from VET processes that are accompanied by the generation of collective excitations of the lower-energy liquid continuum.[18] For convenience, we call these collective excitations "phonons", recognizing that liquids are not periodic solids. The initial VET processes occur primarily in the downward direction, i.e., higher-energy vibration → lower-energy vibrations + phonons. As VET progresses, the bath gradually heats up and eventually thermalizes. In equilibrium, both downward and upward VET dynamically coexist, where upward VET can be represented as phonons + lower-energy vibration → higher-energy vibrations. This process is called phonon up-pumping.[19]

In the rest of this paper, we will describe the ordinary (1D) IR and Raman spectra and vibrational assignments of the four liquids we studied. Then, we will examine and discuss the 3D spectra we obtained.

2. IR-RAMAN SPECTROSCOPY: SIGNALS AND ARTIFACTS

In our measurements, we simultaneously obtained both Stokes and anti-Stokes spectra. The usual practice when this is done is to have the wavenumber (x-axis) be a positive quantity for the Stokes region and a negative quantity for the anti-Stokes region. However, throughout this study, we will be comparing and overlapping Stokes and anti-Stokes spectra. Thus, for convenience, we will make the wavenumbers in both regions positive quantities. When it becomes necessary to distinguish among them, we will use the terms "Stokes wavenumber" and "anti-Stokes wavenumber".

Following an IR pump pulse at t = 0, the time-dependent occupation number of a vibration at frequency ω, $n_\omega(t)$, is given in terms of time-dependent Stokes intensity $I_\omega^{ST}(t)$ and anti-Stokes intensity $I_\omega^{AS}(t)$ as[20]

$$I_\omega^{ST}(t) \propto \omega_L(\omega_L - \omega)^3[n_\omega(t) + 1]\sigma_\omega^R \quad (1)$$

and

$$I_\omega^{AS}(t) \propto \omega_L(\omega_L + \omega)^3 n_\omega(t)\sigma_\omega^R \quad (2)$$

where σ_ω^R is the Raman cross section for transitions at frequency ω when the probe laser frequency is ω_L. The proportionality factors in eqs 1 and 2 depend on the excitation and detection conditions. Our apparatus has been calibrated so the proportionality factors become wavelength-independent and identical in both equations. In the limit that the Raman shifts $\omega_L \pm \omega$ and occupation numbers $n_\omega(t)$ are small, which is approximately the case here, the Stokes spectrum becomes time independent, and the time-dependent occupation numbers are simply $n_\omega(t) = I_\omega^{AS}(t)/I_\omega^{ST}$. However, it is difficult to express 3D spectra in this form because I_ω^{ST} is close to zero in broad regions between vibrational transitions. Thus, instead, we plot only the change in time-dependent anti-Stokes intensities $\Delta I_\omega^{AS}(t)$, where this quantity is equal to the instantaneous anti-Stokes intensity with the ambient temperature background subtracted away. To help the reader account for the I_ω^{ST} factors, we will draw reference I_ω^{ST} Stokes spectra on top of each 3D spectrum.

The bulk temperature jump ΔT created by an IR pulse is typically 0−30 K in our experiments. On the picosecond time scale of the IR-Raman measurements, the T-jump appears static. The T-jump actually decayed by thermal conduction on the 0.1 ms time scale, and the interval between pump pulses was 1 ms.[4] The NM and ACN liquids are mostly thermalized after ∼10 ps, so we stopped our 3D data acquisition at 10 ps. However, from previous studies, we know there may be small amounts of energy trapped in longer-lived excitations, and ACN or NM may not be fully thermalized until 100−200 ps.[15,16]

The magnitude of ΔT is

$$\Delta T = J\alpha/C \quad (3)$$

where J is the IR laser fluence, α is the IR absorption coefficient, and C is the heat capacity, which is approximately constant for small ΔT. When a 3D spectrum was acquired, as the IR pulse was tuned through peaks and valleys of the IR absorption, the IR absorption coefficient varied and ΔT varied in proportion to α. Thus, each pump wavenumber will have a different ΔT, and in order to help the reader account for this effect, we have drawn a reference IR absorption profile in the lower left corner of each 3D spectrum. It should be kept in mind that the relationship of I_ω^{AS} to α and ΔT is rather complicated. Nominally, I_ω^{AS} should

dx.doi.org/10.1021/jp405197g | J. Phys. Chem. B XXXX, XXX, XXX−XXX

increase exponentially with ΔT, but this increase is somewhat offset by the IR-Raman technique's enhanced sensitivity to weaker IR transitions, as explained in the Introduction. Thus, the pump wavenumber dependence of I_ω^{AS} will be more gradual than suggested by the reference IR absorption profiles.

Several kinds of artifacts could be observed in the 3D spectra. By artifacts, we mean optical signals in the anti-Stokes region unrelated to vibrational populations, that decay with the much faster optical dephasing time constants T_2 rather than vibrational population time constants T_1. These artifacts were generated by nonlinear optical processes, and even quite high-order processes are a concern because the pump and probe pulses are intense, the samples are concentrated neat liquids, and the anti-Stokes signals are weak. Thus, nonlinear effects that can be ignored in many pump−probe experiments become significant and sometimes overwhelming in IR-Raman measurements.[4]

The artifacts we see are created by processes that can broadly be described as nonlinear light scattering (NLS).[21] NLS is defined as scattered light at frequencies other than those present in the incident laser pulses. Some nonlinear laser processes produce coherent beams. We have carefully arranged the geometry of our apparatus to minimize the detection of such coherent beams, but in a liquid medium, the scattered light from a coherent signal can be detected and can compete with the anti-Stokes signals. The three most important types of artifacts arise from sum-frequency generation (SFG), via the second-order nonlinear susceptibility $\chi^{(2)}$, which generates signals at $\omega_{IR} + \omega_{vis}$; four-wave mixing (4WM) via $\chi^{(3)}$, which generates signals at $2\omega_{IR} + \omega_{vis}$; and self-phase modulation (SPM) of the Raman probe pulses, which spectrally broadens the probe pulses and which generates signals near zero wavenumbers.

In the SFG literature, where liquid surfaces and interfaces are studied, it is frequently said that $\chi^{(2)}$ vanishes in nonchiral liquids, but that is only true in the dipole approximation.[22] Quadrupole and other higher-order terms in the polarization expansion can lead to weak SFG, even from nonchiral liquids such as NM or ACN. Water is a particularly useful medium for understanding these SFG signals, and using them to characterize the IR and visible laser pulses, since NLS signals from water are especially intense.[23,24] An SFG artifact at $\omega_{IR} + \omega_{vis}$ would appear at the anti-Stokes wavenumber ω_{IR}, which is the same wavenumber as the parent vibrational excitation generated by the IR pump pulses. SFG artifacts appear only near $t = 0$, when the IR and visible pulses are time-coincident.

A 4WM artifact depends on $\chi^{(3)}$, which is nonvanishing in all liquids, so the 4WM artifacts in liquids can be more intense than SFG artifacts. A signal at $2\omega_{IR} + \omega_{vis}$ would appear at the anti-Stokes wavenumber $2\omega_{IR}$, which is generally outside of the range we detect, and should in principle be rejected by our spectrograph. However, because our spectrograph is imperfect, 4WM artifacts can sometimes be observed in anti-Stokes spectra as long decaying tails extending into the 3D spectrum from the higher wavenumber region. The 4WM artifacts are also observed only near $t = 0$.

The SPM artifacts are related to the ubiquitous issue of Rayleigh scattering backgrounds in Raman spectroscopy. These backgrounds are signals in a Raman spectrum that tail off from a maximum at zero wavenumbers. In our Raman system, as in most others, a notch filter was used to suppress Rayleigh scattering. However, when the probe pulses were intense, SPM caused the probe spectrum to broaden, and sometimes this broadened light was transmitted through the notch filter. SPM artifacts look like Rayleigh scattering backgrounds, and are time-independent. The SPM effect can be eliminated by attenuating the probe pulses, but due to the weak signals in our experiments, we run the probe intensity right up to the SPM threshold, and occasionally a laser or sample jet fluctuation will create an SPM artifact. Near $t = 0$, when the pump and probe pulses are time-coincident, the electric fields of the pump pulses enhance SPM of the probe pulses. This type of pump-enhanced SPM artifact also appears as a Rayleigh scattering background, but the pump-enhanced SPM artifact has an intensity maximum at $t = 0$.

3. EXPERIMENTAL SECTION

The experimental apparatus, with a 1 kHz amplified Ti:sapphire laser and dual optical parametric amplifiers (OPAs), has evolved and improved through the years. The most recent version used for the present 3D measurements is diagrammed in Figure 1. It

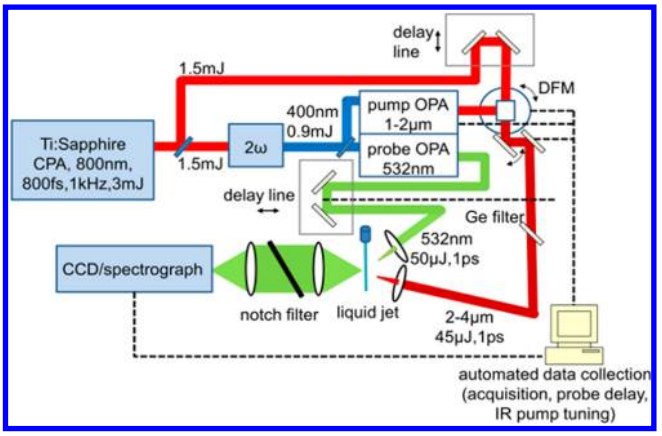

Figure 1. Schematic layout of the 3D IR-Raman spectroscopy apparatus. Key: CPA = chirped-pulse amplifier, OPA = optical parametric amplifier, DFM = difference frequency mixer crystal.

produced IR pump pulses tunable from 3600 to 2150 cm^{-1}, and 532 nm Raman probe pulses. Anti-Stokes and Stokes Raman spectra were simultaneously collected by a spectrograph that covered the range ±3700 cm^{-1}.

A calibrated blackbody source was used to correct for the wavelength-dependent detectivity factors in eqs 1 and 2. The ambient-temperature liquid sample was a cylindrical flowing jet 50 μm in diameter, and the laser beam diameters were about 100 μm. The apparatus time response, which was a consequence of both IR and Raman pulse durations, was about 1 ps. The apparatus spectral resolution, which resulted from the combined spectral bandwidths of the IR and visible pulses and the spectrograph resolution, was about 30 cm^{-1}. These temporal and spectral responses were determined by monitoring spectra of SFG NLS signals from water[23,25] as the time delay was swept.

The important improvement needed for 3D spectra collection is depicted in Figure 1. The IR pump pulses were generated in a KTA (potassium titanyl arsenate) difference-frequency mixing (DFM) crystal, where the inputs were 800 nm Ti:sapphire pulses and tunable pulses in the 0.966−1.12 μm range from one OPA. As the result of the interplay of many factors, it turned out that the ~40 μJ IR pulse energies varied little across this tuning range, so we did not try to normalize the 3D spectra for the wavelength dependence of the IR pulse energy. The OPA (Light Conversion TOPAS-400 ps) had a built-in computer-controlled wavelength scanning capability. Using additional computer-controlled motors, we synchronized the phase-matching rotation of the DFM crystal to the OPA tuning, and corrected for the slight

dx.doi.org/10.1021/jp405197g | J. Phys. Chem. B XXXX, XXX, XXX−XXX

wandering of the IR beam at the sample throughout its tuning range. The IR beam wandering was corrected by a computer-controlled mirror immediately after the DFM crystal that, in calibration runs, was tweaked to maximize the NLS SFG signals from water or finely powdered $LiNbO_3$; this tweaking information was stored in the computer and used during 3D spectra acquisitions.

The NM and ACN were obtained from Sigma-Aldrich, and were used without further purification. The deuterated samples were obtained from Cambridge Isotope Laboratories and were >99.8% deuterated. In order to reduce the time needed for 3D data acquisition, we did not always use the full IR tuning range, but instead, we selected a limited range based on each liquid's IR spectrum. Then, the IR pulse wavenumber was scanned in 50 cm^{-1} increments. At each pump wavenumber, the time delay was swept over the range of 0−10 ps as Raman spectra were acquired.

4. RESULTS

A. IR and Raman Spectra. In order to understand and discuss IR-Raman data, we have found it essential to have at hand plots of the conventional IR and Raman spectra for each sample accompanied by vibrational assignments. Figures 2−5 show

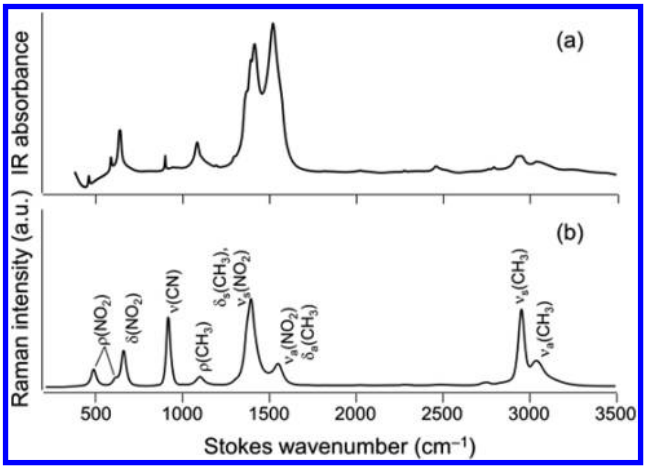

Figure 2. (a) Infrared spectrum of nitromethane (NM) with 4 cm^{-1} resolution. (b) Raman spectrum of nitromethane with assignments, obtained using the picosecond laser. The resolution was 20 cm^{-1}. Adapted from ref 17.

these spectra for NM and ACN. Figures 2−4 are adapted from prior publications,[15,17] and Figure 5 is new. The IR spectra were obtained using FTIR with 4 cm^{-1} resolution, so the observed linewidths were equal to the natural linewidths. The Raman spectra were obtained using picosecond pulses. As a result of the picosecond pulse bandwidth, the Raman resolution was degraded[15] to ∼20 cm^{-1} and frequently this broadened the observed transitions. The spectral assignments for NM and d_3-NM[26−31] and ACN and d_3-ACN[32,33] were taken from prior literature studies.

A few aspects of these spectra are worth mentioning. In the CH-stretch region (∼2900 cm^{-1}) and the CD-stretch region (∼2200 cm^{-1}), the NM spectra are more congested than the ACN spectra. For example, compare some of the sharper ACN IR absorption bands near 3000 cm^{-1} in Figure 4a and near 2200 cm^{-1} in Figure 5a to the corresponding broader NM bands in Figures 2a and 3a. In those regions, spectral assignments are not simple, and even today not entirely conclusive. Nearby or directly underneath the CH-stretch and CD-stretch fundamentals are

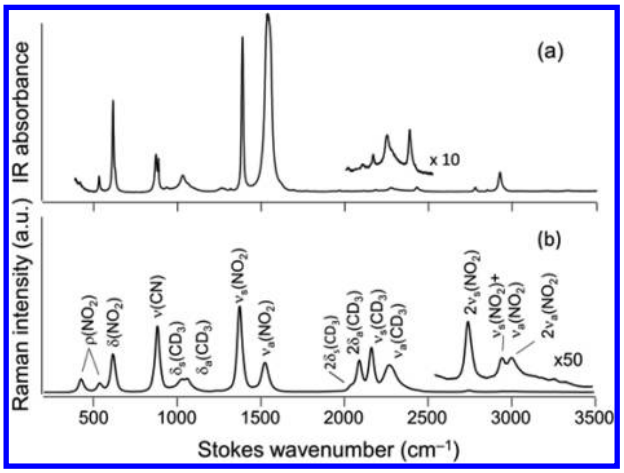

Figure 3. (a) Infrared spectrum of d_3-nitromethane (d_3-NM) with 4 cm^{-1} resolution. (b) Raman spectrum with assignments, obtained using the picosecond laser. Nitro-stretch overtones and combination bands could be seen in the ∼3000 cm^{-1} region. The resolution was 20 cm^{-1}. Adapted from ref 17.

numerous overtones and combinations of the lower-energy modes. Ordinarily, the IR absorption coefficients for these overtones and combinations would be small, but they can borrow intensity from the fundamental transitions. Thus, pumping in this region with IR pulses does not create simple CH-stretch or CD-stretch excitations but rather an admixture of them with lower-energy states. The most well-known example of this effect arises from the 2:1 Fermi resonance between CH-stretch and CH-bend (or CD-stretch and CD-bend), where, as observed in both NM[16,17] and ACN,[14,15] pumping the stretch transition promptly creates bend excitations as well. Another important factor is that, in NM, the nitro-stretches near 1500 cm^{-1} are so close in energy to the CH-bends that they are strongly mixed, and a CH-stretch/nitro-stretch 1:2 resonance is also possible.

With d_3-NM (Figure 3), the CD-bends are downshifted enough to become well-separated from the nitro-stretches, and also from the CN-stretch. However, there is another kind of mixing. The CD-bends near 1100 cm^{-1} are resonant with the methyl rocking $\rho(CD_3)$, which was 1104 cm^{-1} in NM.

In ACN (Figure 4), there is a 2:1 Fermi resonance between $\nu_a(CH_3)$ and $2\delta_a(CH_3)$ but not between $\nu_s(CH_3)$ and $2\delta_s(CH_3)$.[15] As a result, the $\nu_a(CH_3)$ and $\delta_a(CH_3)$ transitions are noticeably broader than $\nu_s(CH_3)$ and $2\delta_s(CH_3)$. The same pattern is seen in d_3-ACN (Figure 5). In ACN, the CN-stretch is an isolated excitation, but in d_3-ACN, the CN-stretch is close to and strongly mixed with the CD-stretch $\nu_a(CD)$.

B. 3D Spectra. The 3D anti-Stokes spectra are shown in Figures 6−9. Since the intensities spanned a wide range, we made the intensity scale logarithmic, as indicated in the color guide in the upper right-hand corner. The diagonals where the parent excitations and SFG NLS artifacts appear are indicated by guide lines in the t = 0 spectra. A Stokes Raman spectrum with vibrational assignments runs along the top of each 3D spectrum. The Raman spectrum provides a reference for the wavenumber dependence of the Raman cross section. An IR absorption spectrum runs along the left side of the 3D spectrum in the lowest panel. The IR spectrum provides a reference for the ΔT dependence on pump wavenumber.

The 3D spectra were rectangular. The x-axis (anti-Stokes Raman wavenumber) range was fixed at 250−4000 cm^{-1}. The aspect ratio was between 3:1 and 5:1, depending on the selected

dx.doi.org/10.1021/jp405197g | J. Phys. Chem. B XXXX, XXX, XXX−XXX

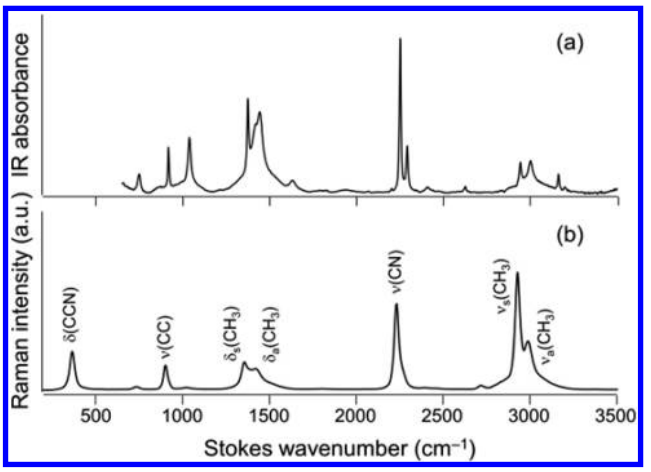

Figure 4. (a) Infrared spectrum of acetonitrile (ACN) with 4 cm^{-1} resolution. (b) Raman spectrum with assignments, obtained using the picosecond laser. The resolution was 20 cm^{-1}. Adapted from ref 15.

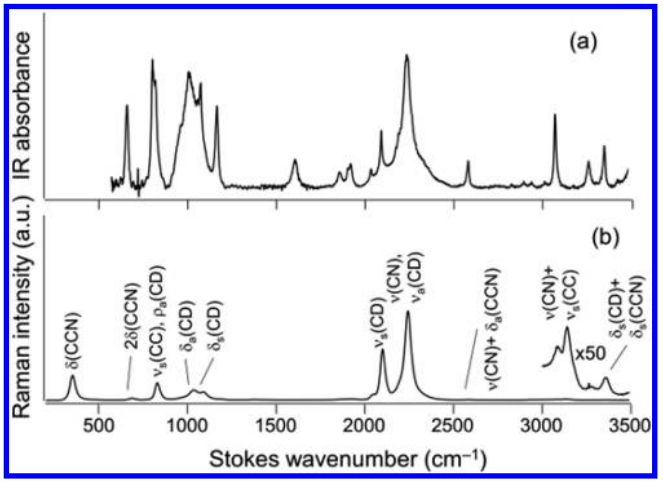

Figure 5. (a) Infrared spectrum of d_3-acetonitrile (d_3-ACN) with 4 cm^{-1} resolution. (b) Raman spectrum with assignments, obtained using the picosecond laser. The resolution was 20 cm^{-1}. Above 2500 cm^{-1}, several overtones and combination bands could be observed, especially those involving ν(CN).

IR wavenumber tuning range. The 3D spectra were quite complicated. Along the diagonal were two fundamental CH-stretch (or CD-stretch) transitions and several combination bands or overtone transitions. Because Raman spectroscopy allows us to simultaneously probe a wide wavenumber region, for every diagonal peak, there were ~10 off-diagonal peaks. Note that, in contrast to 2DIR spectra,[34] where there are $v = 1 \rightarrow 0$ transitions and $v = 0 \rightarrow 1$ transitions on either side of the diagonal, in a multidimensional spectrum where anti-Stokes Raman is used as the probe, only the $v = 1 \rightarrow 0$ transitions are detected.

5. DISCUSSION

Due to the complexity of the 3D spectra, and due to the fact that 3D IR-Raman spectroscopy is in an early stage, in this study, we will limit the discussion to a broad overview. The earlier-time t = 0, 1 ps spectra are used to characterize the nature of the parent excitations, and the subsequent time dependence to characterize each liquid's VET processes.

In a 3D spectrum, the time evolution of the horizontal stripes contains information about how vibrational energy progresses

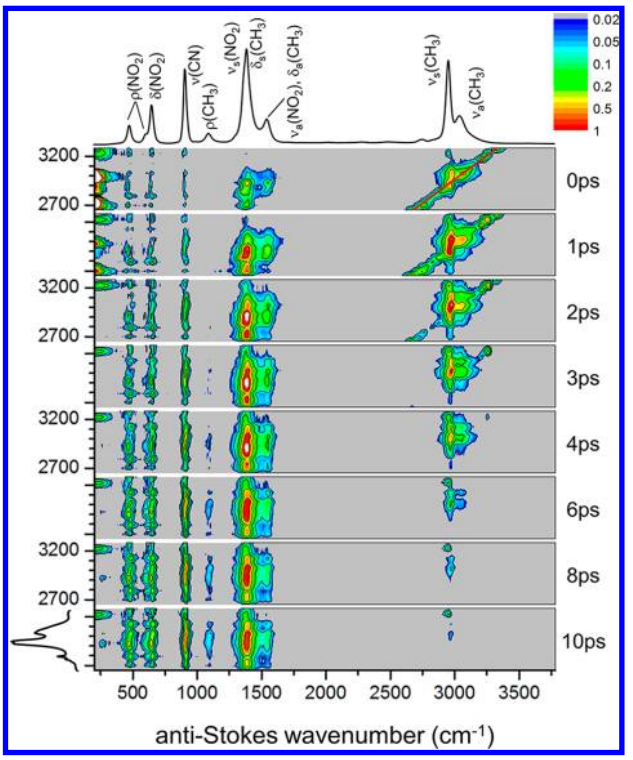

Figure 6. 3D IR-Raman spectrum of nitromethane. A reference Raman spectrum with assignments was drawn above the top panel and a reference IR spectrum to the left of the bottom panel. A reference diagonal was indicated in the top panel. Note the logarithmic intensity scale.

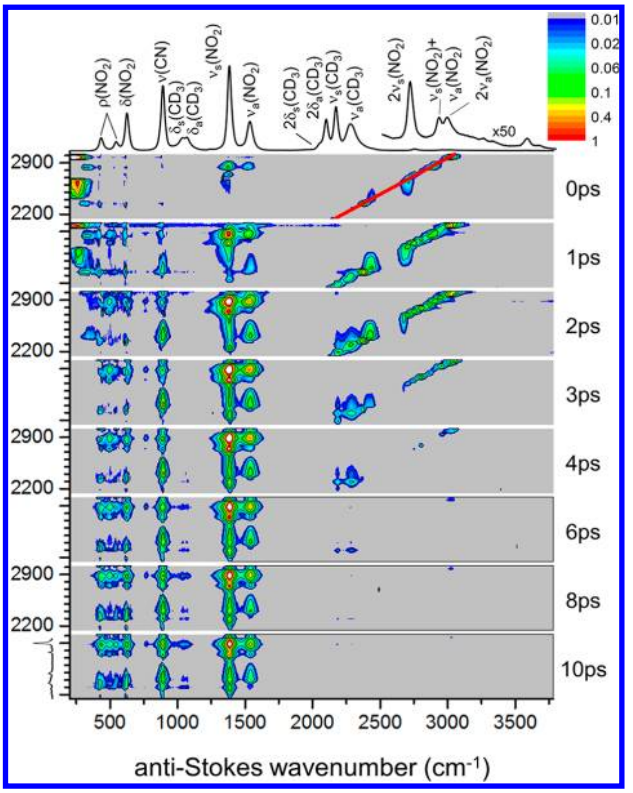

Figure 7. 3D IR-Raman spectrum of d_3-nitromethane.

from a particular excited parent state toward a thermalized state. The time dependence of vertical stripes contains information

dx.doi.org/10.1021/jp405197g | J. Phys. Chem. B XXXX, XXX, XXX−XXX

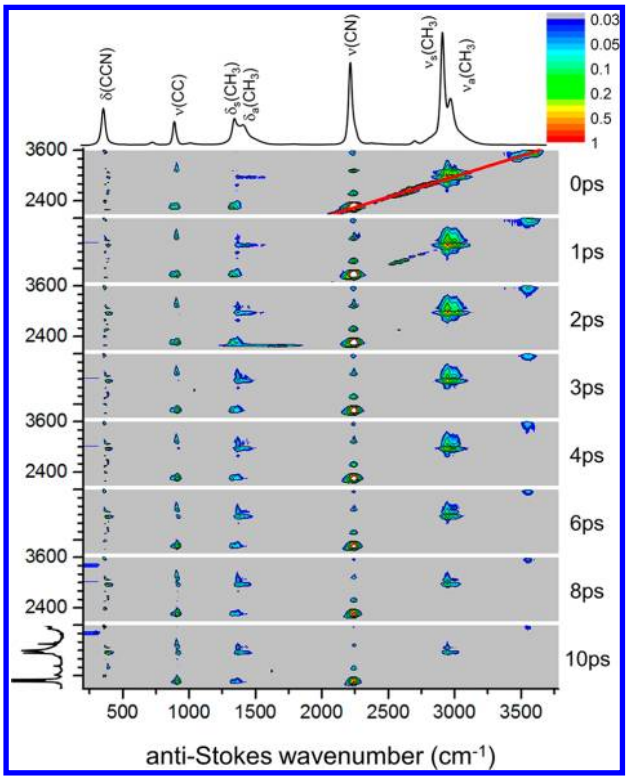

Figure 8. 3D IR-Raman spectrum of acetonitrile.

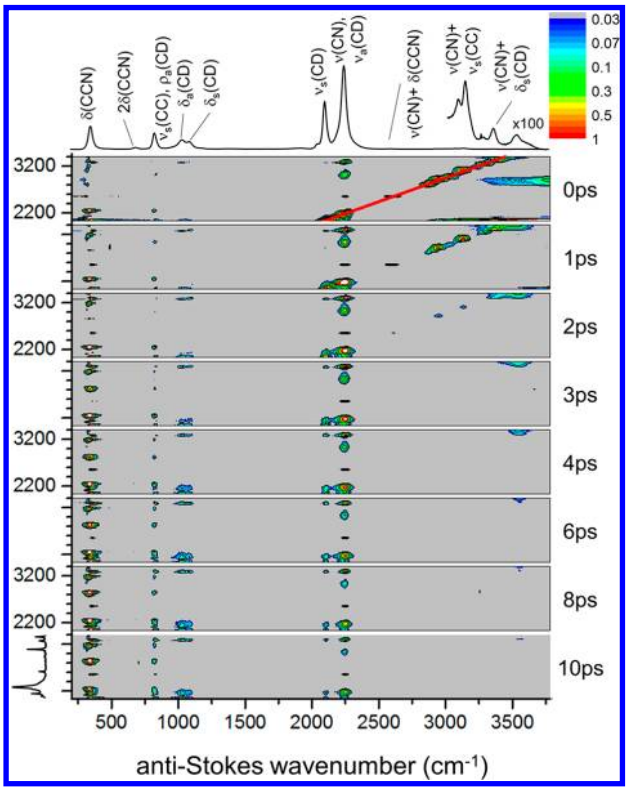

Figure 9. 3D IR-Raman spectrum of d_3-acetonitrile.

about how vibrational population relaxation depends on which parent state was pumped. If a vertical stripe had a uniform intensity at a given instant, it would mean the excitations in that stripe had no memory of which parent state was initially excited. At longer times when the liquid has thermalized, there is no explicit memory of which state was initially excited, except in the limited sense that ΔT depends on the IR absorption coefficient of the parent state. After the liquid thermalizes, vertical stripes in the 3D spectrum would not be expected to be entirely uniform; the intensity variation along a vertical stripe would reflect variations in IR absorption coefficients across the pump tuning range, as described in section 2.

A. Artifacts. The three types of artifacts described above, SFG, 4WM, and SPM, were all observed at one time or another in Figures 6−9. The diagonal signals may include contributions from both parent vibrational populations and SFG artifacts. We can determine if a signal along the diagonal is solely an SFG artifact, because in that case there would be no vibrational population and no anti-Stokes signals in the corresponding horizontal stripe. For example, in Figure 8 at 2500 cm^{-1}, the diagonal signals appear to be purely SFG artifacts.

In Figure 9, we see the strongest effect of 4WM artifacts. These are the stripes running from the far right side of the figure at $t = 0$, 1 ps. These signals are the lower-wavenumber tails of the scattered light from a coherent 4WM signal generated at $2\omega_{IR} + \omega_{vis}$, which in the anti-Stokes spectrum would be peaked off the right-hand side of the figure, at 5800 cm^{-1}.

In Figure 6, we see both types of SPM artifacts. These are the signals at the lowest wavenumbers, below the $\rho(NO_2)$ transitions. They appear as horizontal stripes extending toward zero wavenumber. A time-independent SPM artifact was observed when the IR pump was 3200 cm^{-1}. We evidently exceeded the probe pulse intensity threshold for SPM in that run. At some other IR wavenumbers such as 3000 cm^{-1}, we saw intense SPM artifacts near $t = 0$, which resulted from pump-pulse enhanced SPM of the probe pulse. After 1 ps, these pump-enhanced SPM signals disappeared.

B. Nitromethane. We will first consider the shorter-time (0, 1 ps) NM spectra in Figure 6 as the IR pump pulses were scanned through the CH-stretch region, from 3200 to 2700 cm^{-1}. At 3200 cm^{-1}, well above the nominal CH-stretch absorption, there are no clearly evident absorption bands (Figure 2a), but nonetheless, Figure 6 shows excitations promptly appearing in $\nu(CN)$, $\delta(NO_2)$, and $\rho(NO_2)$. Thus, there must be a combination-band transition near 3200 cm^{-1} that combines the character of these three modes. This example illustrates the ability of shorter-time 3D IR-Raman spectroscopy to detect and characterize weak combination-band transitions. At 3100 cm^{-1}, there is a diagonal signal but very little population in the lower-wavenumber modes, so the diagonal signal at 3100 cm^{-1} was primarily an SFG artifact. At 3000 cm^{-1}, where the IR pulses were near the absorption maximum of $\nu_a(CH_3)$, the 3D spectrum shows that both $\nu_a(CH_3)$ and $\nu_s(CH_3)$ were excited. This is a consequence of spectral overlap between the $\nu_a(CH)$ absorption peak and the higher-energy tail of $\nu_s(CH_3)$. This 3000 cm^{-1} excitation condition also promptly produced all lower-wavenumber vibrations except 607 cm^{-1} $\rho(NO_2)$. At 2900 cm^{-1}, pumping into the absorption maximum of $\nu_s(CH_3)$, we saw little $\nu_a(CH_3)$ but we did see all lower-wavenumber vibrations except $\rho(NO_2)$, with 1402 cm^{-1} (symmetric CH-bend/nitro-stretch) especially prominent. At 2800 cm^{-1}, we promptly saw all lower-wavenumber vibrations except 1562 cm^{-1} (asymmetric CH-bend/nitro-stretch) and 607 cm^{-1} (nitro-bend). At 2700 cm^{-1}, something interesting happened. A great deal of excitation appeared at 1402 cm^{-1}, even though there was little CH-stretch excitation, which suggests that we pumped and observed the first overtone of the 1402 cm^{-1} CH-bend/nitro-stretch transition.

dx.doi.org/10.1021/jp405197g | J. Phys. Chem. B XXXX, XXX, XXX−XXX

Looking at the longer-time spectra in Figure 6, we saw NM proceeding toward a thermalized state. It is interesting that $\rho(CH_3)$ at 1104 cm^{-1} was never excited at shorter times, indicating that this excitation is practically decoupled from the other normal modes. It is possible that the later-time excitation of $\rho(CH_3)$, as the NM approaches thermalization, results solely from phonon up-pumping of lower-energy excitations.

Looking at the intensity profiles along the vertical stripes of the lower-wavenumber bands, recall these spectra are plotted using a logarithmic intensity scale, which flattens out the pump wavenumber dependence of the intensity. Once the NM has thermalized, one would expect these intensity profiles to approximately track the IR absorption spectrum in Figure 2a, which has a maximum at 2968 cm^{-1}, a much weaker maximum at 3050 cm^{-1}, and little intensity above 3150 cm^{-1} or below 2850 cm^{-1}. In fact, this is not quite what is observed. All the lower-wavenumber signals at longer delay times (except $\rho(CH_3)$ do have maxima near 2968 and 3050 cm^{-1}, but they also have excess populations below (e.g., 2750 cm^{-1}) and above (e.g., 3200 cm^{-1}) the CH-stretch resonances. Populating the lower-wavenumber excitations by pumping in this region surely indicates that combination bands are being excited, and the magnitude of the lower-wavenumber population results from the enhanced sensitivity of IR-Raman spectroscopy to weaker IR absorption transitions.

C. d_3-Nitromethane. With d_3-NM (Figure 7), we will first consider the shorter-time spectra at t = 0, 1 ps, as the IR pulses were tuned from 3000 to 2150 cm^{-1}. As shown in Figure 3b (and at the top of Figure 7), between 3000 and 2400 cm^{-1}, the only transitions in this deuterated solvent were overtones and combinations of nitro-stretches. By tuning through this range, the 3D spectrum confirmed the assignments we proposed in Figure 3b. When the band near 3000 cm^{-1} that we proposed to be $2\nu_a(NO_2)$ was excited, only $\nu_a(NO_2)$ was observed. Similarly, at 2900 cm^{-1}, proposed to be $\nu_a(NO_2) + \nu_s(NO_2)$, both $\nu_a(NO_2)$ and $\nu_s(NO_2)$ were observed. At 2700 cm^{-1}, proposed to be $2\nu_s(NO_2)$, only $\nu_s(NO_2)$ was observed.

At IR pump wavenumbers where CD-stretches were excited, the dominant daughter excitations generated by VET were the ~1400 cm^{-1} nitro-stretches, and there was hardly any excitation of the ~1100 cm^{-1} CD-bends.

Comparing Figures 6 and 7 results in a quite interesting observation about CH-stretch relaxation of NM compared to CD-stretch relaxation of d_3-NM. The usual expectation would be that CH-stretch pumping would primarily generate CH-bend excitations, and CD-stretch pumping would primarily generate CD-bend excitations.[2] However, in NM, the nitro-stretch excitations are resonant with the CH-bend states, whereas, in d_3-NM, the nitro-stretch excitations are in the region between CD-stretches and CD-bends. Thus, the following question can be posed: Is the relaxation of a CH-stretch or CD-stretch excitation on the methyl group more likely to involve the methyl group itself or the adjacent nitro group? With NM, it is impossible to tell because there is so much coupling between the nitro-stretch and methyl-bend, but with d_3-NM, it is clear that CD-stretch relaxation to the adjacent nitro group is much more efficient than to bends on the same methyl group.

D. ACN. ACN (Figure 8) was scanned from 3600 to 2150 cm^{-1}. The vertical stripes in the ACN spectra were more patchy than with NM (Figure 6). This is a reflection that the ACN IR absorption spectrum in the pumped region (Figure 4a) is less congested than NM (Figure 2a). In the first 0, 1 ps, with 3600 cm^{-1} pumping, well above CH-stretch absorbances, a diagonal signal was seen, but it was not entirely SFG artifact, since the corresponding horizontal stripe shows some excited-state populations of ν(CN) and δ(CCN). Since ν(CN) is 2253 cm^{-1}, the most likely origin would be a combination with $\delta_s(CH_3)$ (1312 cm^{-1}), but the shorter-time 3D spectrum in Figure 8 with 3600 cm^{-1} pumping showed very little excitation near 1312 cm^{-1} and quite a bit at 379 cm^{-1}. Thus, this excitation seemingly involved ν(CN) with at least one and probably multiple quanta (up to 3) of 379 cm^{-1} δ(CCN) bending excitations. Moving the pump wavenumber lower, nothing much was seen until the CH-stretches came into resonance. The higher-energy CH-stretches produced mainly ν(CN) and ν(CC), whereas the lower-energy CH-stretches produced mainly CH-bends. Pumping the region just below the CH-stretches (2800−2400 cm^{-1}) produced little vibrational excitation except near 2600 cm^{-1} where a small amount of ν(CN) and δ(CCN) appeared, indicating that 2600 cm^{-1} IR pulses pumped the ν(CN) + δ(CCN) combination. Nothing much was seen below 2400 cm^{-1} until the 2253 cm^{-1} ν(CN) transition was pumped, and at that point, we promptly observed $\delta_s(CH_3)$ and ν(CC). Looking at the longer-time data, the primary daughter excitations from CH-stretch pumping and from CN-stretch pumping were CH-bends and ν(CC).

E. d_3-ACN. The d_3-ACN spectrum in Figure 9 was scanned from 3400 to 2000 cm^{-1}. At the highest wavenumbers 3400−2600 cm^{-1}, the 3D spectra confirm the assignments given in Figure 5b and at the top of Figure 9, where we have indicated combination bands of ν(CN) with δ(CCN), ν_s(CC), and δ_s(CD). When we pump the CD-stretch and CN-stretch regions, the other prompt excitations were small amounts of CD-bend, CC-stretch, and CCN-bend. Looking at the longer-time data, we see that when the CD-stretch and CN-stretch excitations decayed they produced CD-bends, CC-stretches, and CCN-bends.

6. CONCLUSIONS

The 3D spectra were quite complicated due to the multitude of off-diagonal peaks. With this 3D method, the cross-peaks at shorter delay times revealed the nature of the initial excitation. Especially when the initial excitation was a combination band or overtone, and even when those bands were very weak in the IR absorption spectrum, the 3D spectra did a remarkable job of characterizing which excitations were produced when those weak bands were pumped. Looking at longer-time spectra, it was easy to characterize the vibrational energy relaxation processes and identify which daughter vibrations were created from different parent excitations.

AUTHOR INFORMATION

Corresponding Author

*E-mail: dlott@illinois.edu.

Notes

The authors declare no competing financial interest.

ACKNOWLEDGMENTS

The research described in this study is based on work supported by the Office of Naval Research under award N00014-11-1-0418, the National Science Foundation under award DMR-09-55259, and the US Air Force Office of Scientific Research under award FA9550-09-1-0163.

REFERENCES

(1) Iwaki, L. K.; Dlott, D. D. Three-Dimensional Spectroscopy of Vibrational Energy Relaxation in Liquid Methanol. *J. Phys. Chem. A* **2000**, *104*, 9101−9112.

(2) Laubereau, A.; Kaiser, W. Vibrational Dynamics of Liquids and Solids Investigated by Picosecond Light Pulses. *Rev. Mod. Phys.* **1978**, *50*, 607−665.

(3) Laubereau, A.; von der Linde, D.; Kaiser, W. Direct Measurement of the Vibrational Lifetimes of Molecules in Liquids. *Phys. Rev. Lett.* **1972**, *28*, 1162−1165.

(4) Deàk, J. C.; Iwaki, L. K.; Rhea, S. T.; Dlott, D. D. Ultrafast Infrared-Raman Studies of Vibrational Energy Redistribution in Polyatomic Liquids. *J. Raman Spectrosc.* **2000**, *31*, 263−274.

(5) Iwaki, L. K.; Deàk, J. C.; Rhea, S. T.; Dlott, D. D. Vibrational Energy Redistribution in Polyatomic Liquids: Ultrafast IR-Raman Spectroscopy. In *Ultrafast Infrared and Raman Spectroscopy*; Fayer, M. D., Ed.; Marcel Dekker: New York, 2001; pp 541−592.

(6) Pein, B. C.; Dlott, D. D. Vibrational Energy and Molecular Thermometers in Liquids: Ultrafast IR-Raman Spectroscopy. In *Ultrafast Infrared Vibrational Spectroscopy*; Fayer, M. D., Ed.; CRC Press Taylor & Francis Group: Boca Raton, FL, 2013; pp 269−304.

(7) Dlott, D. D. Vibrational Energy Redistribution in Polyatomic Liquids: 3d Infrared-Raman Spectroscopy. *Chem. Phys.* **2001**, *266*, 149−166.

(8) Laubereau, A.; Kehl, G.; Kaiser, W. Picosecond Spectroscopy of Molecular Vibrations in Liquids. A Vibrational Bottleneck in Ethanol. *Opt. Commun.* **1974**, *11*, 74.

(9) Graener, H.; Laubereau, A. Ultrafast Vibrational Energy Transfer of Polyethylene Investigated with Picosecond Laser Pulses. *Chem. Phys. Lett.* **1987**, *133*, 378−380.

(10) Seilmeier, A.; Kaiser, W. Ultrashort Intramolecular and Intermolecular Vibrational Energy Transfer of Polyatomic Molecules in Liquids. In *Ultrashort Laser Pulses and Applications*; Kaiser, W., Ed.; Springer Verlag: Berlin, 1988; Vol. *60*, pp 279−315.

(11) Iwaki, L. K.; Dlott, D. D. Ultrafast Vibrational Energy Redistribution within C-H and O-H Stretching Modes of Liquid Methanol. *Chem. Phys. Lett.* **2000**, *321*, 419−425.

(12) Pein, B. C.; Sun, Y.; Dlott, D. D. Unidirectional Vibrational Energy Flow in Nitrobenzene. *J. Phys. Chem. A* **2013**, DOI: 10.1021/jp3127863.

(13) Deàk, J. C.; Iwaki, L. K.; Dlott, D. D. High Power Picosecond Mid-Infrared Optical Parametric Amplifier for Infrared-Raman Spectroscopy. *Opt. Lett.* **1997**, *22*, 1796−1798.

(14) Deàk, J. C.; Iwaki, L. K.; Dlott, D. D. When Vibrations Interact: Ultrafast Energy Relaxation of Vibrational Pairs in Polyatomic Liquids. *Chem. Phys. Lett.* **1998**, *293*, 405−411.

(15) Deàk, J. C.; Iwaki, L. K.; Dlott, D. D. Vibrational Energy Redistribution in Polyatomic Liquids: Ultrafast IR−Raman Spectroscopy of Acetonitrile. *J. Phys. Chem. A* **1998**, *102*, 8193−8201.

(16) Deàk, J. C.; Iwaki, L. K.; Dlott, D. D. Vibrational Energy Redistribution in Polyatomic Liquids: Ultrafast IR-Raman Spectroscopy of Nitromethane. *J. Phys. Chem. A* **1999**, *103*, 971−979.

(17) Shigeto, S.; Pang, Y.; Fang, Y.; Dlott, D. D. Vibrational Relaxation of Normal and Deuterated Liquid Nitromethane. *J. Phys. Chem. B* **2008**, *112*, 232−241.

(18) Kenkre, V. M.; Tokmakoff, A.; Fayer, M. D. Theory of Vibrational Relaxation of Polyatomic Molecules in Liquids. *J. Chem. Phys.* **1994**, *101*, 10618−10629.

(19) Dlott, D. D.; Fayer, M. D. Shocked Molecular Solids: Vibrational up Pumping, Defect Hot Spot Formation, and the Onset of Chemistry. *J. Chem. Phys.* **1990**, *92*, 3798−3812.

(20) Graener, H.; Zürl, R.; Hofmann, M. Vibrational Relaxation of Liquid Chloroform. *J. Phys. Chem.* **1997**, *101*, 1745−1749.

(21) Terhune, R. W.; Maker, P. D.; Savage, C. M. Measurements of Nonlinear Light Scattering. *Phys. Rev. Lett.* **1965**, *14*, 681−684.

(22) Shen, Y. R. *The Principles of Nonlinear Optics*; Wiley: New York, 1984.

(23) Deàk, J. C.; Rhea, S. T.; Iwaki, L. K.; Dlott, D. D. Vibrational Energy Relaxation and Vibrational Spectral Diffusion in Liquid Water and Deuterated Water. *J. Phys. Chem. A* **2000**, *104*, 4866−4875.

(24) Wang, Z.; Pang, Y.; Dlott, D. D. Hydrogen-Bond Disruption by Vibrational Excitations in Water. *J. Phys. Chem. A* **2007**, *111*, 3196−3208.

(25) Pakoulev, A.; Wang, Z.; Dlott, D. D. Vibrational Relaxation and Spectral Evolution Following Ultrafast OH Stretch Excitation of Water. *Chem. Phys. Lett.* **2003**, *371*, 594−600.

(26) Wells, A. J.; Wilson, E. B. Infra-Red and Raman Spectra of Polyatomic Molecules XIII. Nitromethane. *J. Chem. Phys.* **1941**, *10*, 314−318.

(27) McKean, D. C.; Watt, R. A. Vibrational Spectra of Nitromethanes and the Effects of Internal Rotation. *J. Mol. Spectrosc.* **1976**, *61*, 184−202.

(28) Hill, J. R.; Moore, D. S.; Schmidt, S. C.; Storm, C. B. Infrared, Raman, and Coherent Anti-Stokes Raman Spectroscopy of the Hydrogen/Deuterium Isotopomers of Nitromethane. *J. Phys. Chem.* **1991**, *95*, 3037−3044.

(29) Courtecuisse, S.; Cansell, F.; Fabre, D.; Petite, J. P. Comparative Raman Spectroscopy of Nitromethane-H_3, Nitromethane-D_3, and Nitroethane up to 20 GPa. *J. Chem. Phys.* **1998**, *108*, 7350−7355.

(30) Shkurinov, A.; Jonusauskas, G.; Rullière, C. Vibrational Spectrum of Liquid Nitromethane Revisited Using Polarization-Sensitive Coherent Anti-Stokes Raman Scattering (CARS) Spectroscopy. *J. Raman Spectrosc.* **1994**, *25*, 359−364.

(31) Miller, P. J.; Block, S.; Piermarini, G. J. Effects of Pressure on the Vibrational Spectra of Liquid Nitromethane. *J. Phys. Chem.* **1989**, *93*, 462−466.

(32) Herzberg, G. *Molecular Spectra and Molecular Structure II. Infrared and Raman Spectra of Polyatomic Molecules*; Van Nostrand Reinhold: New York, 1945.

(33) Pace, E. L.; Now, L. J. Infrared Spectra of Acetonitrile and Acetonitrile-D_3. *J. Chem. Phys.* **1968**, *49*, 5317−5325.

(34) Hamm, P.; Zanni, M. T. *Concepts and Methods of 2D Infrared Spectroscopy*; Cambridge University Press: Cambridge, U.K., 2011.